5th International Energy Conversion Engineering Conference and Exhibit (IECEC)
25 - 27 June 2007, St. Louis, Missouri

AIAA 2007-4722

Multiphase Free-Piston Stirling Engine for Solar-Thermal-Electric Power Generation Applications

Artin Der Minassians* and Seth R. Sanders†

EECS Department, University of California at Berkeley, Berkeley, CA, 94720, USA

This paper addresses the design, fabrication, and test of a three-phase free-piston Stirling engine system. The system is conceived as an integral part of a solar-thermal-electric power generation technology suitable for distributed deployment. Medium temperature (180 °C to 250 °C) heat is delivered to the Stirling engines by means of non-imaging solar concentrators and an integrated electromagnetic alternator converts the mechanical output power of the system into electricity. Dynamical formulation of a multiphase Stirling engine system is presented with a modal analysis for the three-phase system, and shows the potential of the system to be self-starting. Design and fabrication of low loss diaphragm pistons, etched and woven-wire screen heat exchangers, and plastic flexures, as the main components of the system, are outlined. Furthermore, two main test methodologies for system assessment are discussed, and measurement results are presented and compared with design calculations. Test results are convincing for the flexure, heat exchanger flow friction losses, and gas spring hysteresis loss. However, experimental data reveal that gas spring hysteresis loss is an important dissipation phenomenon and should be carefully addressed in the free-piston Stirling engine design.

I. Introduction

Due to their high relative cost, solar electric energy systems have yet to be exploited on a widespread basis. It is believed in the energy community that a technology similar to photovoltaic (PV), but offered at about $1/W would lead to widespread deployment at residential and commercial sites. There has been an ongoing effort on low-cost solar-thermal-electric power generation technology in the EECS department at UC Berkeley over the past few years. The proposed energy conversion system is conceived to convert solar power into electricity in three stages: solar power to heat, heat to mechanical power, and mechanical power to electricity. Low-concentration non-imaging solar collectors are capable of delivering thermal power at temperatures in the range of 180 °C to 250 °C. without having to track the sun.[1] A non-tracking system avoids the costs and maintenance issues associated with tracking collectors with high concentration ratios. Thus, a non-imaging solar collector is a very suitable component to serve as the first energy conversion stage of the proposed system.

A heat engine, in the proposed system, is utilized to convert the delivered heat by the solar concentrator into mechianical power. Among possible choices for thermodynamic cycles, work has focused on the Stirling cycle initially. One potential advantage of the Stirling cycle is the possibility of using ambient air as the working fluid, and thus avoiding issues with long-term containment. Further, recent success in demonstrating very low temperature-differential engines is also compelling.[2] The Stirling engine converts moderate-temperature heat to electricity by way of integrated electric generation in the system conceived here. However, the use of low-temperature heat limits the theoretical maximum thermodynamic efficiency achievable by the heat engine, which limits the overall system efficiency. This disadvantage, however, can be compensated by lower costs in materials and in reduced maintenance. We take the view that cost effectiveness of solar electric technologies should be judged by output power per dollar rather than by efficiency or other merits.[3]

In this paper we discuss the analysis, design, fabrication, and the experimental results of a three-phase Stirling engine system. This system is the first prototype which serves as a test rig for assessing the accuracy of the implemented models during the design process.

*Ph.D. Candidate, EECS Department, 205 Cory Hall, Berkeley, CA, 94720. E-mail: artin@eecs.berkeley.edu
†Professor, EECS Department, 518 Cory Hall, Berkeley, CA, 94720. E-mail: sanders@eecs.berkeley.edu

II. Dynamical Modeling and Analysis

Figure 1 shows the schematic diagram of an N-phase Stirling engine system. An isothermal model is the simplest formulation for thermodynamic behavior of a Stirling engine,[4] and will be used to understand the nominal system dynamics. For the i-th Stirling cycle that operates in this system, pressure of the working fluid, p_i, is given by

$$p_i = (MR) \Big/ \left(\frac{V_e^{nom} - A_P x_i}{T_h} + \frac{V_c^{nom} + A_P x_{i+1}}{T_k} + \frac{V_k}{T_k} + \frac{V_r}{T_r} + \frac{V_h}{T_h} \right) \quad i = 1, \cdots, N \tag{1}$$

where M is the mass of the working fluid, R is the ideal gas constant, V_e^{nom} and V_c^{nom} are, respectively, the nominal volumes of expansion and compression spaces, A_P is the cross-sectional area of each piston, x_i is the displacement of the i-th piston, T_h and T_k are, respectively, the temperatures of the heater and cooler in each Stirling engine, and finally V_h, V_r, and V_k are the free volumes of the heater, regenerator, and cooler, respectively. Assuming an adiabatic regenerator and a linear temperature profile across this component between the cold temperature and the hot temperautre, the mean effective regenerator temperature, T_r, can then be expressed as[4]

$$T_r = \frac{T_h - T_k}{\ln (T_h / T_k)} \tag{2}$$

Consider each piston to be a mass-spring subsystem (m_P, K_P), with linear viscous friction (B_P), that is coupled to its two adjacent neighbors through the working gas modeled by Eq. (1). Hence, the following system of differential equations represents the nonlinear dynamical behavior of the multiphase system.

$$A_P (p_{i-1} - p_i) - B_P \dot{x}_i - K_P x_i = m_P \ddot{x}_i \quad i = 1, \cdots, N \tag{3}$$

In steady state operation, the pistons have a symmetrically skewed-phase oscillatory motion and, of course, the efficiency and output power of each engine, and hence the entire system, is a function of the phase delay between volume variation of compression and expansion spaces.[4] Simulated waveforms for steady state operation are shown in figure 2b.

To assess feasibility of self-starting, a linearized system model can be derived by linearizing Eq. (3) at the origin ($x_i = 0,\ i = 1, \cdots, N$) as shown in Eq. (4). Note that the N-th engine is followed by the first engine in a multiphase system loop.

$$\ddot{x}_i = \left(\frac{A_P}{m_P} \frac{\alpha}{T_h} \right) x_{i-1} - \left(\frac{A_P}{m_P} \frac{\alpha}{T_h} + \frac{A_P}{m_P} \frac{\alpha}{T_k} + \frac{K_P}{m_P} \right) x_i + \left(\frac{A_P}{m_P} \frac{\alpha}{T_k} \right) x_{i+1} - \left(\frac{B_P}{m_P} \right) \dot{x}_i \quad i = 1, \cdots, N \tag{4}$$

where

$$\alpha = (MR) \Big/ \left(\frac{V_e^{nom}}{T_h} + \frac{V_c^{nom}}{T_k} + \frac{V_k}{T_k} + \frac{V_r \ln (T_h / T_k)}{T_h - T_k} + \frac{V_h}{T_h} \right)^2 A_P \tag{5}$$

For the linearized system, if the pistons had no damping ($B_P = 0$), the eigenvalues would be located along the $j\omega$-axis at thermal equilibrium ($T_h = T_k$), and hence, the slightest temperature difference between compression and expansion spaces would drive the two eigenvalues, which correspond to the forward three-phase operating mode,[3] to the right half plane (RHP, unstable region). However, with damping present ($B_P \neq 0$) all eigenvalues fall in the left half plane (LHP, stable region) at thermal equilibrium. As T_h increases, the two eigenvalues start to migrate toward the unstable region. Beyond a certain temperature, depending on the engine parameters, the equilibrium becomes unstable and the system exhibits self-starting behavior. Simulation of the dynamic behavior shows that a slight perturbation in one phase drives the system away from its unstable equilibrium, figure 2a, until the system locks itself into a limit cycle due to the loading on the pistons and system internal dissipations, figure 2b.

III. System Design and Fabrication

Ambient pressure air has been selected initially as the working fluid of the Stirling engines in order to minimize the maintenance requirements of the system. The engine parameters are tabulated in table 1. Each engine ideally (based on the Schmidt analyis[4]) will produce more than 115 W output mechanical power

Table 1. Engine thermodynamic design parameters.

Working fluid	Ambient pressure air
Operating frequency	50 Hz
Operating temperautres	T_h: 420 K T_k: 300 K
Expansion and compression spaces	Volume: 78.5 cm^3
Heater and Cooler	Housing volume: 78.5 cm^3 Screen porosity: 64%
Regenerator	Housing volume: 78.5 cm^3 Screen porosity: 53%
Pistons	Diameter: 10 cm Stroke: 2 cm
Indicated output power	115.6 W

with 28% efficiency at 50 Hz. However, there are a number of loss contributors in a Stirling engine system, including fluid flow friction at the heat exchangers (heater, cooler, and regenerator), thermal ineffectiveness in these components, mechanical friction losses, and static heat loss, among others, that will be discussed hereafter. A summary of the Stirling engine system design has been presented in figure 3 in form of a power flow diagram, which incorporates all the losses and inefficiencies that were considered at the design stage.

A. Heat Exchangers

Fluid flow through heat exchangers is an irreversible phenomenon that requires "pumping power" to overcome the viscous friction involved. The required pumping power is supplied as a fraction of the engine's available mechanical output power and, hence, is a source of loss. A good heat exchanger should provide enough surface area to transfer the required heat to the working fluid with the least possible temperature drop and, at the same time, introduce the least possible flow friction (or pressure drop) loss. A well-designed heat exchanger maintains a reasonable balance between temperature and pressure drops. Figure 4 shows the fabricated heat exchanger screens and the heater housing. The power resistors attached to the outside perimeter of the heater act as the heating elements. It is worth noting that the regenerator is a stack of woven-wire screens with circular cross-section wire, whereas the heater and cooler are stacks of etched screens (not woven) with square cross-section etched wire. Furthermore, in addition to its conventional sealing task, the o-ring is designed to separate the hot and cold sides of each engine in order to minimize the static heat loss from heater to cooler.

For flow friction, several empirical correlations, that are obtained from experiments on various fluids and operating conditions, have been compared in Ref. 5 and updated in Ref. 6. All considered correlations are for steady flow conditions, except the one by Tanaka.[7] On the other hand, the predicted efficiency based on the Tanaka correlation is actually exceeded in experimental measurements reported in Ref. 7. Furthermore, since the working fluid conditions reported on by Tanaka (e.g., temperature, pressure, fluid type, Reynolds number) fit in the range of conditions for the Stirling engine design discussed here, we have relied on the Tanaka correlations in our design computations.

B. Diaphragm pistons

Mechanical friction is virtually eliminated by replacing moving pistons by diaphragms, and by realizing bearings with flexures. Thus, losses associated with surface-to-surface sliding friction and lifetime limitations associated with mechanical wear are avoided. As a further consequence, lack of static friction enables the engine system to self-start upon application of heat. In addition, there is no emphasis on difficult sealing requirements that have plagued conventional crank-mechanism Stirling designs.

Figure 5 shows the fabricated three-phase Stirling engine system. Corrugated diaphragms, figure 6, are fabricated by casting silicone in custom designed wax molds. Nylon cantilevers are used as flexures for each pair of two pistons that rigidly connect the expansion space of one engine to the compression space of the

other. These flexures have to be designed to be very stiff in the axial and radial directions, but with low loss and low stiffness for angular motion. This low angular stiffness combined with the mass of each piston assembly defines a pure displacement resonant frequency of the system at about 11.9 Hz in this design.

C. Actuator

One of the three magnetic actuators that was fabricated for the three-phase Stirling system is shown in figure 7. Magnets are connected to the jaw that is indicted in figure 5 and move as the pistons oscillate. Therefore, as a generator or motion sensor, when the pistons (and hence magnets) move, an alternating magnetic flux links the coils which, in turn, induces voltage on the winding terminals. On the other hand, as an actuator, when alternating current flows through the windings, the resulting electromagnetic force pushes the magnet pair back and forth depending on the direction of the current flow.

Actuators are connected to a variable frequency three-phase inverter. Hence, in addition to driving the system in heat pump regime, each Stirling engine may be driven (as an alpha-type machine) in pure displacement or compression modes using two actuators only, if mechanically separated from the other two phases. The latter two driving modes are particularly useful while assessing the fluid flow and gas compression losses, respectively.

IV. System Assessment and Experimental Results

The following methodologies have been implemented in assessment of the prototype:

- *Ring-Down Test*

  A ring-down test is an appropriate way for estimating the various parameters of a simple dynamical system. The system is displaced from its equilibrium and is released. By looking at the rate and type of the envelope (exponential for viscous friction or linear for dry friction,) one can translate it into important system parameters such as natural frequency, quality factor and damping factor, which are then used to estimate the power loss.

- *Calorimetric Transient Test*

  Any loss within a component generates heat and, therefore, has the potential of increasing the component's temperature. In a calorimetric test, the temperature transient behavior is observed while the component runs in the desired operating conditions. An estimation algorithm is then utilized to estimate the amount of the generated heat (i.e., the loss within that component). This algorithm is based upon a thermal model that is developed for the component and its surrounding environment. It should be noted that accurate knowledge of a component's thermal mass is a key point in this test. Since obtaining a priori accurate values of thermal resistance is very difficult, equivalent thermal dissipation is extracted from the temperature transient characteristic by the estimation process.

A. Fluid Flow Friction

We found the ring-down test to be the most appropriate method to evaluate frictional losses. Figure 8 shows the ring-down test for one of the three Nylon cantilever hinges. In order to assess the feasibility of the designed cantilever, none of the diaphragms (nor the heat exchangers) are linked in this experiment. By observing the damped oscillations in figure 8, one can conclude that the natural frequency of the mass-spring system is about 3.7 Hz. This is a function of the cantilever stiffness and the equivalent moving mass. Quality factor is about 26.7 which is an indication of minimal losses in the designed Nylon pivot.

Table 2 tabulates resonant frequency, f_{res}, quality factor, Q, and damping factor, B, of the ring-down tests that were carried out for various cases to estimate the contribution of each component on the overall system behavior, and in particular, power dissipation. The Nylon hinge stiffness is about 350 N/m based on a separate measurement. Therefore, the equivalent moving mass is about 0.64 kg, which enables calculation of the dissipated power loss at design excursion of 1 cm. This data is tabulated in column P_{loss}^{meas} and the estimated dissipation at the 50 Hz operating frequency is listed in column P_{loss}^{est}.

The Nylon cantilever hinge, the diaphragms, and the magnetic stuffness of the actuator are the three components that contribute to the stiffness of the mass-spring system with the actuator stiffness being

Table 2. Summary of the ring-down tests carried out on the prototype. On each row the cross sign indicates which components were included in the test. P, D, K, H, R, and C refer to pivot, diaphragm, cooler, heater, regenerator, and C-core (actuator's laminated steel core shown in figure 7), respectively.

P	D	K	H	R	C	f_{res}, Hz	Q	B, N.s/m	P_{loss}^{meas} at f_{res}, W	P_{loss}^{est} at 50 Hz, W
×						3.7	26.7	0.56	0.02	2.75
×	×	×				7.5	10.8	2.78	0.31	13.72
×	×	×	×			7.5	8.9	3.42	0.38	16.89
×	×	×	×	×		7.5	6.3	4.80	0.53	23.8
×					×	10.2	65.4	0.62	0.13	3.06
×	×	×			×	11.9	19.3	2.49	0.70	12.28
×	×	×	×		×	11.9	17.4	2.76	0.77	13.61
×	×	×	×	×	×	11.9	9.5	5.07	1.42	25

Table 3. Comparison of the measured flow friction data with designed values for heater and regenerator.

f, Hz	$P_{H,\,loss}^{meas}$, W	$P_{H,\,loss}^{calc}$, W	$P_{R,\,loss}^{meas}$, W	$P_{R,\,loss}^{calc}$, W
7.5	0.07	0.04	0.15	0.65
11.9	0.07	0.13	0.65	1.7
50	3.17	4.3	11.4	29.8

dominant which basically sets the frequency of the displacement mode operation of the system to about 11.9 Hz.

We can infer the fluid flow loss contribution of the heater and the regenerator at two frequencies (i.e., 7.5 Hz and 11.9 Hz) from table 2. A comparison of the measured data with design values, table 3, signifies that the flow friction correlations suggested by Tanaka[7] for oscillating flow are reliable and even conservative. Hence, using such reliable correlations one can be confident that the fabricated machine will not suffer from excessive flow friction.

B. Gas Spring Hysteresis

Since the thermodynamic process that occurs in a gas spring is not perfectly reversible, there is a loss associated with gas springs. Ref. 4 offers an approximate calculation for gas spring hysteresis that matches our experimental results with excellent accuracy.

A calorimetric transient test proved to be an appropriate method for measuring the losses asociated with gas spring hysteresis. As previously mentioned, 30 Hz is the resonant frequency of the system in pure compression mode, as confirmed by a frequency response test. In order to observe the effect of the heat exchanger on gas spring hysteresis, four different conditions have been considered and tested as tabulated in table 4. In each case, we observed a slightly different resonant frequency for the compression mode that is due to the different volume of gas that is enclosed by the engine chamber. As one may expect, the measured data confirms that by decreasing the working gas volume (adding more screens inside the engine,) the gas

Table 4. Comparison of measured and calculated gas hysteresis (compression) losses in various conditions. The number in the left three columns indicate the fraction of corresponsing heat exchanger screens that is in place.

Heater	Cooler	Regen.	f, Hz	Stroke, mm	P_{comp}^{meas}, W	P_{comp}^{calc}, W
0%	0%	0%	28.2	12	2	2.3
50%	50%	0%	29.2	12	2.6	2.6
100%	100%	0%	29.6	13	3.7	3.7
50%	50%	50%	30	6	0.7	0.7

spring stiffness increases which, in turn, raises the resonant frequency.

In table 4 the measured gas spring hysteresis loss has been compared with the suggested formulation in Ref. 4. This result confirms the accuracy of the calculation and provides a reliable basis for estimation of the compression losses that plays a crucial role in the operation of free-piston Stirling engines.

C. Heat Pump Operation

By driving all three actuators with a balanced symmetrical three-phase power supply, the system operates as a heat pump. Figure 9 shows the temperature variation for both cold and hot sides of a single unit of the three-phase Stirling engine. The system operated in heat pump regime for about 53 minutes during which temperatures of the hot and cold sides separated from their initial thermal equilibrium in two opposite directions. Actuators are tuned off at $t = 53$ minutes, which allows the temperatures to converge back to their equilibrium.

D. Engine Operation

At steady state, as shown in figure 2b, the phase delay between the two pistons of each Stirling engine is intended to be 120 degrees. This condition translates into a large compression ratio (about 45%) for the working fluid inside the engine chamber. The gas spring hysteresis loss, on the other hand, is quadratically proportional to the compression ratio.[4] Hence, it turns out that the gas spring hysteresis loss would be more than 300 W, and thus is very significant for the fabricated system. This loss actually surpasses the nominal output power of the engines. Therefore, it reveals that the gas compression loss is an important dissipation phenomenon and should be carefully addressed in the free-piston Stirling engine design as it hindered the operation of the test system in engine mode.

V. Conclusion

The design, fabrication, and test of a three-phase free-piston Stirling engine system were discussed. As an integral part of a solar-thermal-electric power generation technology, a Stirling engine system was designed to operate with medium-temperature heat input that is generated by non-imaging solar concentrators. Dynamical formulation of a multiphase Stirling engine system was presented with a modal analysis for the three-phase system that highlighted the self-starting potential of the system. The measurement results were presented and compared with design calculations. Tests confirmed convincing results for heat exchanger flow friction losses and for gas spring hysteresis loss. However, it was revealed that gas spring hysteresis loss was an important dissipation phenomenon and should be carefully addressed in the free-piston Stirling engine design as it hindered the operation of the fabricated system.

Acknowledgments

The authors would like to extend their gratitude to the National Science Foundation (award #ECS-0424462), for the financial support of the research presented in this paper. Also, they would like to thank Ben Lake and Warner Carlisle of the Engineering Research Support Organization (ERSO) Machine Shop for their tremendous help in the design and fabrication of the prototype.

References

[1]Welford, W. T. and Winston, R., *High Collection Nonimaging Optics*, Academic Press, San Diego, CA, 1989.

[2]Senft, J. R., *An Introduction to Low Temperature Differential Stirling Engines*, Moriya Press, River Falls, WI, 5th ed., 2002.

[3]Der-Minassians, A., Aschenbach, K. H., and Sanders, S. R., "Low-Cost Distributed Solar-Thermal-Electric Power Generation," *Proceedings of SPIE*, Vol. 5185, 2004, pp. 89–98, Invited Paper.

[4]Urieli, I. and Berchowitz, D. M., *Stirling Cycle Engine Analysis*, Adam Hilger Ltd, Bristol, 1984.

[5]Thomas, B., "Evaluation of 6 Different Correlations for the Flow Friction Factor of Stirling Engine Regenerators," *Proceedings of the 34th Intesociety Energy Conversion Engineering Conference*, 1999.

[6]Thomas, B. and Pittman, D., "Update on the Evaluation of Different Correlations for the Flow Friction Factor and Heat Transfer of Stirling Engine Regenerators," *Proceedings of the 35th Intesociety Energy Conversion Engineering Conference*, Vol. 1, 2000, pp. 76–84.

[7]Tanaka, M., Yamashita, I., and Chisaka, F., "Flow and Heat Transfer Characteristics of the Stirling Engine Regenerator in an Oscillating Flow," *JSME International Journal*, Vol. 33, series II, No. 2, 1990, pp. 283–289.

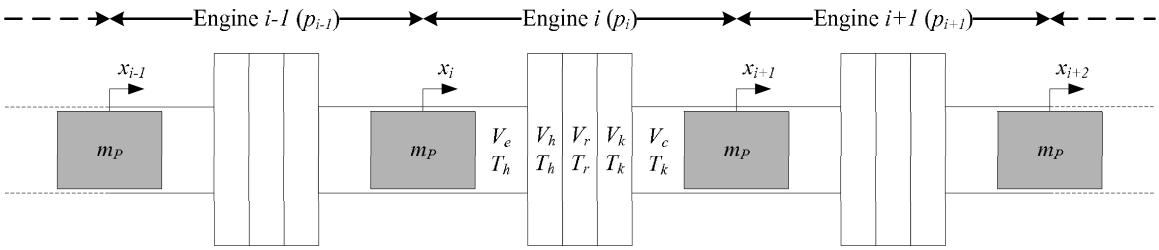

Figure 1. Schematic diagram of a multiphase Stirling engine system.

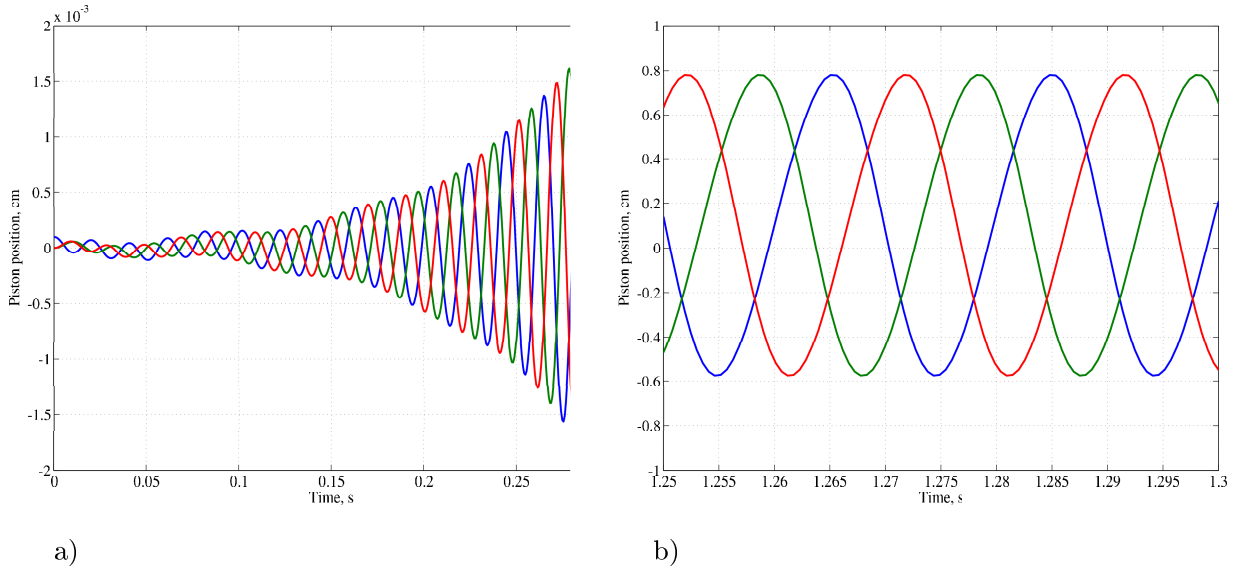

Figure 2. Simulated displacements of the three phases for the designed three-phase Stirling engine system. a) System develops its motion starting from a slight perturbation, indicating potential for self-start. b) After startup, system reaches its three-phase steady state operating condition.

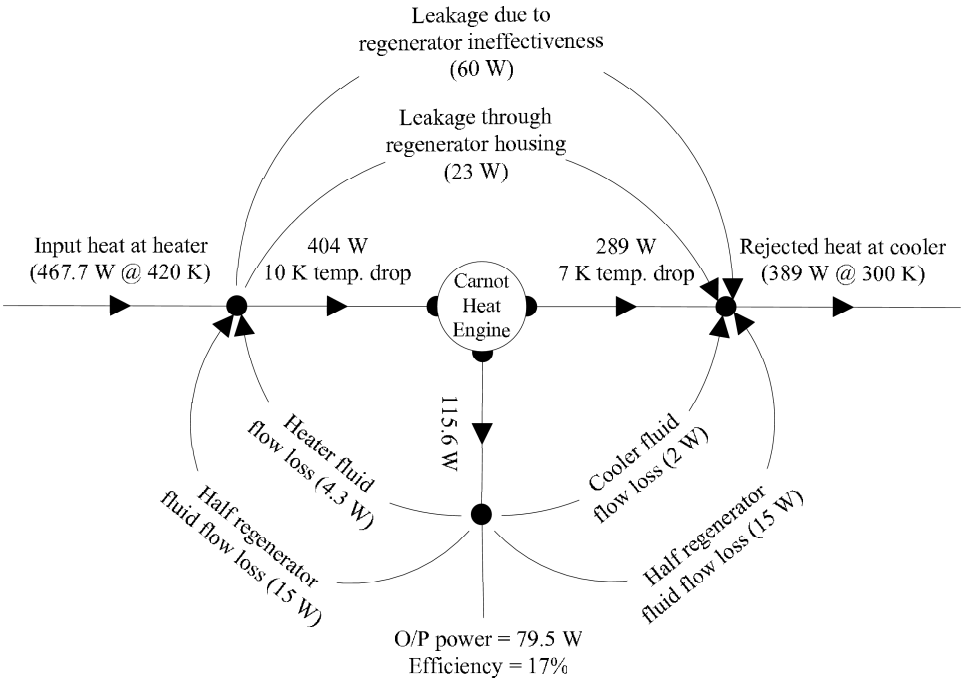

Figure 3. Power balance diagram of the designed Stirling engines.

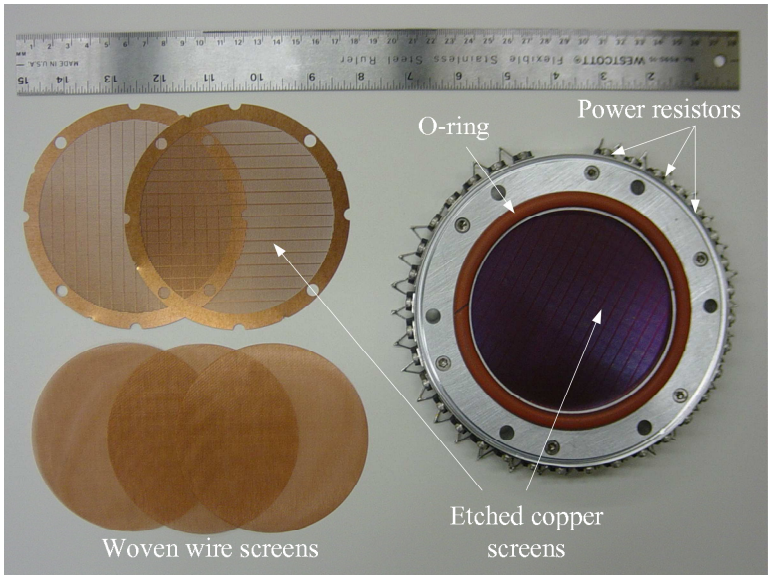

Figure 4. Fabricated heat exchanger frame and the screens.

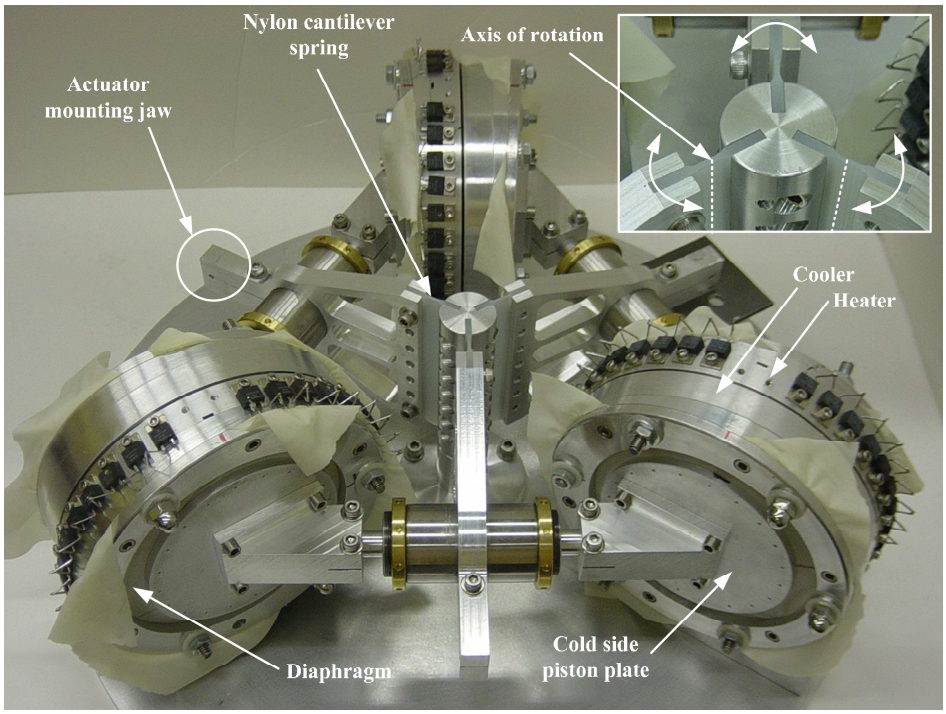

Figure 5. Fabricated three-phase Stirling engine system. Photograph taken before custom corrugated silicone diaphragms were fabricated and installed.

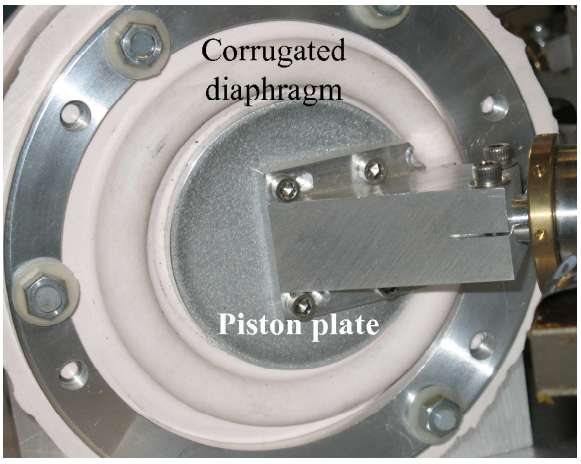

Figure 6. Close-up view of the fabricated diaphragm with one ring of corrugation.

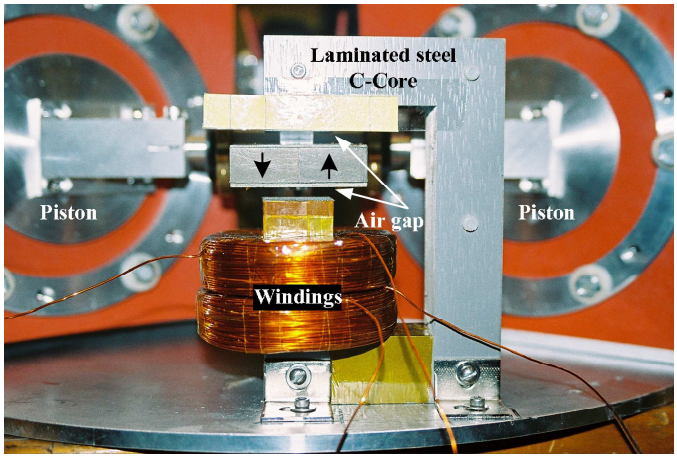

Figure 7. Fabricated magnetic actuator (control circuitry not shown).

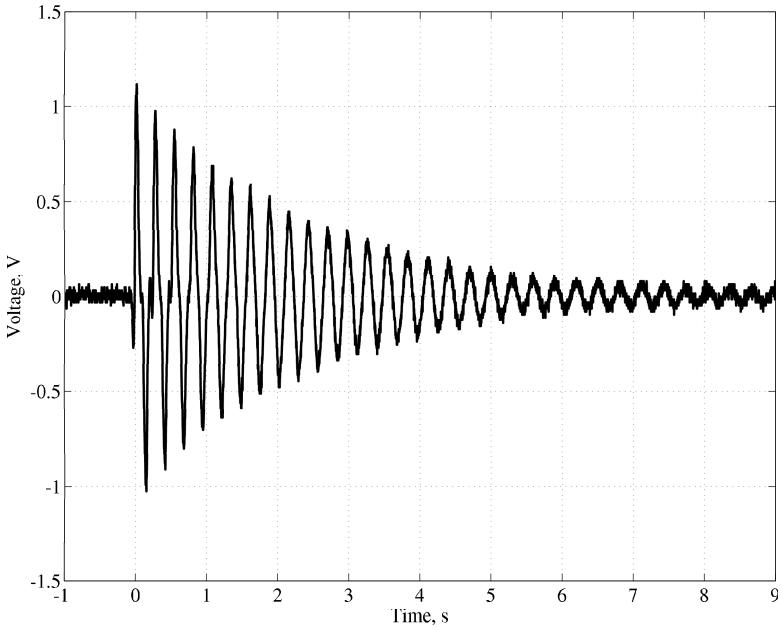

Figure 8. Ring-down characteristic of the Nylon cantilever hinge.

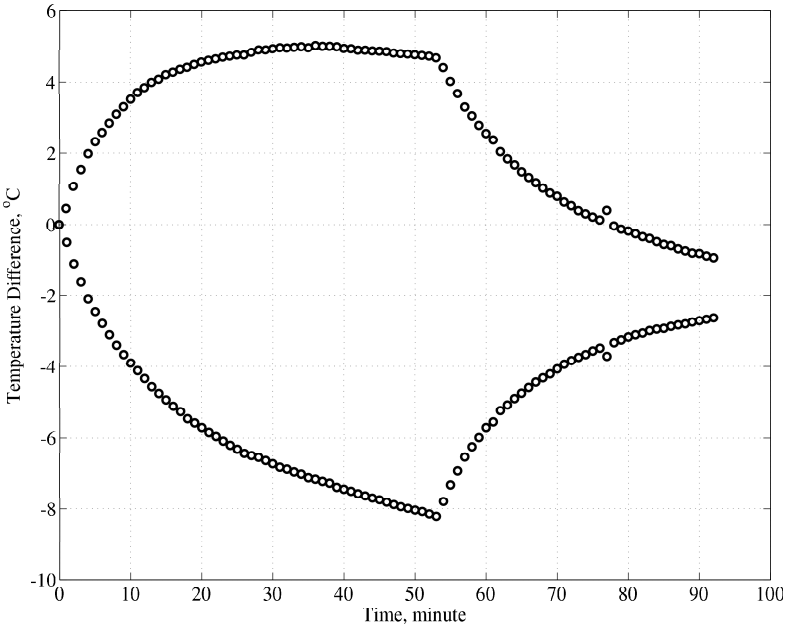

Figure 9. Temperature variation of the hot and cold sides of one Stirling engine during the heat pump regime.